

## Gate-controlled linear magnetoresistance in thin Bi<sub>2</sub>Se<sub>3</sub> sheets

B. F. Gao, P. Gehring, M. Burghard, and K. Kern

Citation: *Appl. Phys. Lett.* **100**, 212402 (2012); doi: 10.1063/1.4719196

View online: <http://dx.doi.org/10.1063/1.4719196>

View Table of Contents: <http://apl.aip.org/resource/1/APPLAB/v100/i21>

Published by the [American Institute of Physics](#).

---

### Related Articles

Ultra-high hole mobility exceeding one million in a strained germanium quantum well  
*Appl. Phys. Lett.* **101**, 172108 (2012)

On the estimation of the magnetocaloric effect by means of microwave technique  
*AIP Advances* **2**, 042120 (2012)

Parallel-leaky capacitance equivalent circuit model for MgO magnetic tunnel junctions  
*Appl. Phys. Lett.* **101**, 162404 (2012)

Influence of Fe segregation at grain boundaries on the magnetoresistance of Sr<sub>2</sub>Fe<sub>1+δ</sub>MoO<sub>6</sub> polycrystals  
*J. Appl. Phys.* **112**, 073925 (2012)

Angular-dependences of giant in-plane and interlayer magnetoresistances in Bi<sub>2</sub>Te<sub>3</sub> bulk single crystals  
*Appl. Phys. Lett.* **101**, 152107 (2012)

---

### Additional information on *Appl. Phys. Lett.*

Journal Homepage: <http://apl.aip.org/>

Journal Information: [http://apl.aip.org/about/about\\_the\\_journal](http://apl.aip.org/about/about_the_journal)

Top downloads: [http://apl.aip.org/features/most\\_downloaded](http://apl.aip.org/features/most_downloaded)

Information for Authors: <http://apl.aip.org/authors>

## ADVERTISEMENT



ACCELERATE COMPUTATIONAL CHEMISTRY BY 5X.  
TRY IT ON A FREE, REMOTELY-HOSTED CLUSTER.

[LEARN MORE](#)

## Gate-controlled linear magnetoresistance in thin Bi<sub>2</sub>Se<sub>3</sub> sheets

B. F. Gao (高波),<sup>1,a),b)</sup> P. Gehring,<sup>1,a)</sup> M. Burghard,<sup>1</sup> and K. Kern<sup>1,2</sup>

<sup>1</sup>Max Planck Institute for Solid State Research, Heisenbergstrasse 1, D-70569 Stuttgart, Germany

<sup>2</sup>Institute de Physique de la Matière Condensée, Ecole Polytechnique Fédérale de Lausanne, CH-1015 Lausanne, Switzerland

(Received 13 February 2012; accepted 22 April 2012; published online 21 May 2012)

We explore the emergence of linear magnetoresistance in thin Bi<sub>2</sub>Se<sub>3</sub> sheets upon tuning the carrier density using a back gate. With increasingly negative gate voltage, a pronounced magnetoresistance of  $\sim 100\%$  is observed, while the associated B-field dependence changes from quadratic to linear. Concomitantly, the resistance-versus-temperature curves evolve from metallic to semiconductor-like, and increasingly strong weak anti-localization behavior is manifested. Analysis of the magnetoresistance data reveals two contributions, namely from the bulk conduction band and from a state inside the bulk gap. The latter is responsible for the linear magnetoresistance and likely represents the topologically protected surface state. © 2012 American Institute of Physics. [<http://dx.doi.org/10.1063/1.4719196>]

Linear magnetoresistance (LMR), first discovered about 100 years ago in Bi,<sup>1</sup> has been observed in a wide range of materials, albeit the underlying mechanism can be quite different.<sup>2–9</sup> Recently, LMR has been reported for topological insulators (TIs), a class of materials possessing an insulating bulk state combined with a topologically protected conducting surface state (TSS).<sup>10–12</sup> Various layered materials including Bi<sub>2</sub>Se<sub>3</sub>, Bi<sub>2</sub>Te<sub>3</sub>, and Bi<sub>1–x</sub>Sb<sub>x</sub> have been identified as three-dimensional topological insulators (3D TIs) with the aid of angle-resolved photoemission spectroscopy (ARPES).<sup>13–19</sup> Further hints have been gained from charge transport and scanning tunneling microscopy (STM) studies, in the form of weak anti-localization,<sup>20</sup> Aharonov-Bohm oscillations,<sup>21,22</sup> as well as Shubnikov-de Haas oscillations<sup>23,24</sup> and related quantum oscillation phenomena.<sup>25–28</sup> Examples of topological materials in which LMR has been detected are Bi<sub>2</sub>Se<sub>3</sub> and Bi<sub>2</sub>Te<sub>3</sub>,<sup>23,29</sup> semimetal YPtBi,<sup>30</sup> as well as the silver-based compounds Ag<sub>2</sub>Te and Ag<sub>2</sub>Se.<sup>31</sup> In case of the prototypical TI Bi<sub>2</sub>Se<sub>3</sub>, LMR has been observed under high magnetic fields applied to 100 nm thick nanoribbons and attributed to the topological surface states.<sup>29</sup> Furthermore, it has been found that Bi<sub>2</sub>Se<sub>3</sub> thin films are able to exhibit LMR down to a thickness of 6 nm, below which a weak negative magnetoresistance emerges.<sup>32</sup> In this letter, we demonstrate the possibility to tune the magnetoresistance characteristics of Bi<sub>2</sub>Se<sub>3</sub> by electrostatically tuning the carrier concentration. Under large negative gate potential, a MR in the order of 100% can be achieved in this manner, a finding that is relevant for magnetic field sensor applications. We assign the LMR observable under such condition to predominant charge transport through TSS. This suggests LMR as a possible fingerprint of TSS in charge transport experiments, thus complementing the widely employed ARPES measurements.

Thin plates of Bi<sub>2</sub>Se<sub>3</sub> were synthesized by a catalyst-free vapor transport method.<sup>33</sup> In a typical experiment, 200 mg of ultrapure Bi<sub>2</sub>Se<sub>3</sub> was placed inside a 2.5 cm diameter quartz tube in the hot zone of a tube furnace, and silicon wafers covered with 300 nm of SiO<sub>2</sub> in the downstream zone (10–12 cm away from the source). Prior to heating, the quartz tube was repeatedly evacuated to a base pressure below 10<sup>–4</sup> mbar and purged with ultrapure Ar to remove the residual oxygen. Then the Ar-flow was set to a constant value of 50 sccm, and the furnace heated to the synthesis temperature of 590 °C at which it was kept for 5–10 min, followed by cooling down under Ar atmosphere. The chemical composition of the product was confirmed by transmission electron microscopy (TEM) and Raman spectroscopy. The TEM analysis revealed the top and bottom surface of the Bi<sub>2</sub>Se<sub>3</sub> platelets to be (0001) facets, while their side faces correspond to (01 $\bar{1}$ 0) facets. Moreover, from the  $\langle 1\bar{1}00 \rangle$  and  $\langle 11\bar{2}0 \rangle$  diffraction peaks, a lattice constant  $a$  of 3.98 Å  $\pm$  0.13 Å (average over 8 different flakes) was calculated, slightly smaller than the previously reported value of 4.14 Å.<sup>34</sup> This difference may originate from a sizeable amount of selenium vacancies in the present samples. The Raman spectra, acquired with a 633 nm laser beam, displayed modes at 131 and 173 cm<sup>–1</sup>, which can be attributed to the E<sub>g</sub> and A<sub>1g</sub> modes of bulk Bi<sub>2</sub>Se<sub>3</sub>, respectively.<sup>35</sup> For the electrical transport studies, Cr/Au electrodes were defined using standard e-beam lithography. To reduce the contact resistance, the exposed contact regions were etched for 6 min in diluted HCl directly before the metal deposition, with the aim of removing the surface oxide (mainly Bi<sub>2</sub>O<sub>3</sub>).

The two- and four-terminal MR of an approximately 10 nm thick platelet is shown as a function of applied (negative) gate voltage in Figs. 1(a) and 1(b), respectively. At the measurement temperature of T = 40 K, the most pertinent features could be observed. For the highest negative gate voltage (V<sub>g</sub> = –100 V), a significant MR of  $\sim 80\%$  is reached. The same MR magnitude was reproducibly observed for nine other samples with thicknesses ranging between 10 and 30 nm. In the lower gate voltage regime ( $|V_g| < 40$  V), the MR curves display a quadratic B-field

<sup>a)</sup>Authors to whom correspondence should be addressed. Electronic addresses: bo\_f\_gao@mail.sim.ac.cn and p.gehring@fkf.mpg.de.

<sup>b)</sup>Current address: Shanghai Institute of Microsystem and Information Technology, Chinese Academy of Science, 865 Changning Road, 200050 Shanghai, China.

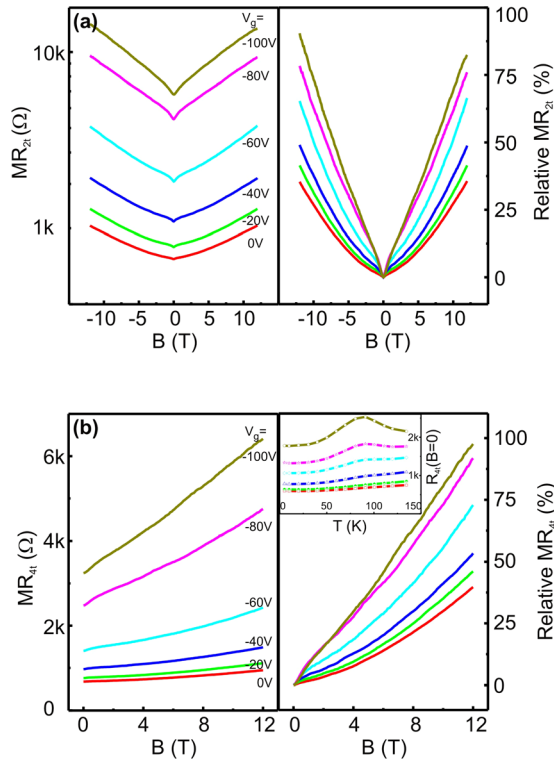


FIG. 1. (a) Two-terminal magnetoresistance of a  $\sim 10$  nm thick  $\text{Bi}_2\text{Se}_3$  sheet at 40 K and at different back gate voltages. The left panel shows the absolute values, and the right the relative magnetoresistance defined as  $(R(B) - R(B=0))/R(B=0)$ . (b) Four-terminal magnetoresistance of the sample at 40 K for different back gate voltages. In left panel, the absolute values are plotted, in the right panel the relative values. In all cases, the Hall contribution was removed from the raw data. Inset: Resistance vs. temperature curves of the sample measured at different gate voltages.

dependence, in accordance with the previous reports.<sup>36</sup> This dependence is characteristic of Lorentz deflection of charge carriers, which can be described by Kohler's rule<sup>37</sup>

$$R(B)/R(B=0) \approx 1 + (\mu B)^2, \quad (1)$$

where  $\mu$  is the carrier mobility. With increasingly negative gate voltage, a transition from quadratic to linear B-field dependence occurs. It is noteworthy that at all gate voltages, the region around  $B=0$  deviates from the linear dependence as a consequence of the weak anti-localization effect,<sup>20,36</sup> which is most pronounced at  $V_g = -100$  V.

The trend from quadratic to linear B-field dependence is obvious from both the two- and four-terminal data, evidencing that the LMR cannot be related to contact resistance. In order to unravel its origin, we measured the temperature dependence of resistance at different gate voltages. As exemplified in the inset of Fig. 1(b) for the above sample, with increasingly negative gate voltage the resistance increases, which is suggestive of reduced carrier concentration. It can furthermore be seen that the  $R$  vs.  $T$  curves exhibit metallic behavior up to  $V_g = -40$  V, while a resistance peak appears at more negative gate voltages. A reasonable explanation for the peak is that two components contribute to the charge transport, with the first one showing normal metallic behavior and the second one thermally activated behavior.<sup>38</sup> While the latter behavior is plausibly connected to the thermal excitation of carriers to the bottom of the conduction band, the

metallic component can be ascribed to a state inside the bulk gap. Although there is good evidence that this state is the topological surface state (see further below), it is termed "gap state" in the following evaluation of the resistance peak.

Fig. 2(a) depicts a set of MR curves measured on the above sample at different temperatures and fixed  $V_g = -100$  V. It is apparent that with decreasing temperature, the curves become more linear. In Fig. 2(b), the corresponding zero field resistance is plotted as a function of temperature. For fitting the curves, we write the total conductance  $G_t$  of the sample as

$$G_t(T) = G_i(T) + G_b(T), \quad (2)$$

where  $G_i$  is the conductance of the gap state, and  $G_b$  is the conductance associated with the bulk conduction band.<sup>37</sup> We furthermore assume that  $G_i$  is given by

$$G_i(T) = 1/(A + BT), \quad (3)$$

where  $A$  accounts for the static disorder scattering and  $B$  introduces electron-phonon coupling.<sup>39</sup> The thermally activated bulk conductance can be written as

$$G_b(T) = n_{b0} e^{-\Delta/T} e\mu = 1/(R_{b0} e^{\Delta/T}), \quad (4)$$

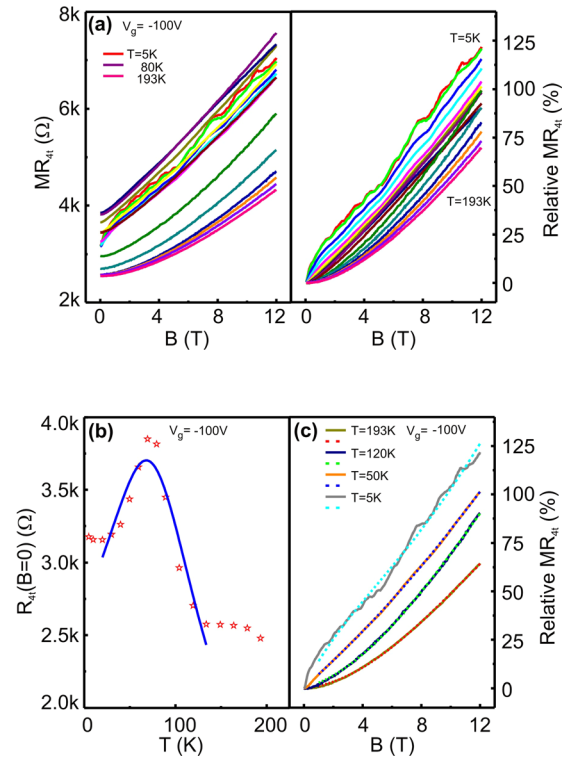


FIG. 2. (a) Four-terminal magnetoresistance of the same sample as in Fig. 1 measured between 5 and 193 K at fixed  $V_g = -100$  V. Left panel: absolute values; right panel: relative values. (b) Resistance at zero B-field measured as a function of temperature with  $V_g$  fixed at  $-100$  V. Fitting (solid line) of the raw data (stars) reveals a thermally activated behavior. (c) Fits (dashed lines) of the raw magnetoresistance curves (solid lines) recorded at four different temperatures. Fitting was performed using the parallel conduction model involving a bulk conduction band and a topological surface state contribution.

where the fitting parameter  $\Delta$  defines the energy gap between the Fermi level and the bottom of the bulk conduction band, and  $G_{b0}$  is the high temperature conductance of the bulk state. The fit of the data in Fig. 2(b) yields  $\Delta = 369.9$  K,  $R_{b0} = 290.7 \Omega$ ,  $A = 2665.3 \Omega$ , and  $B = 18.42 (\Omega/K)$ . The extracted gap size  $\Delta$  is significantly larger than the measurement temperature in Figs. 1(a) and 1(b) ( $T = 40$  K), indicating that under this condition, the bulk conduction band contribution to the transport is strongly suppressed. In fact, based upon the above fitting values, one obtains  $R_b(T = 40 \text{ K}) = 3.0 \text{ M}\Omega$  and  $R_i(T = 40 \text{ K}) = 3.4 \text{ k}\Omega$ . It follows that the bulk resistance exceeds the gap state resistance by approximately three orders of magnitude and is even larger than the total magnetoresistance measured at the highest B-field (12 T). Accordingly, at low temperature, the gap state is expected to dominate the charge transport and thus impart the observed linear magnetoresistance behavior. The poor agreement between the fit and measured data at lowest temperatures ( $T < 20$  K) is attributable to electron-electron interaction.<sup>40</sup>

Under the assumption that the gap state and the bulk conduction band are characterized by a linear and quadratic B-field dependence, respectively, the total magnetoresistance is obtained as

$$R_t(B) = R_i(B) \cdot R_b(B) / (R_i(B) + R_b(B)), \quad (5)$$

where  $R_b(B)$  and  $R_i(B)$  are the bulk and gap state resistance. Each component can be expressed by

$$R_b(B) = R_b(0) + \alpha B^2 \quad (6)$$

and

$$R_i(B) = R_i(0) + \beta B. \quad (7)$$

As  $R_i(0)$  and  $R_b(0)$  are interrelated fitting parameters, only three fitting parameters remain. The fits yield the mobility of the bulk charge carriers  $\mu_b = \sqrt{\alpha/R_b(0)}$  and the bulk carrier density  $n_b = 1/(R_b(0)e\mu_b F)$ , where  $F = W/L = 3$  represents the sample width divided by length. The curve fits in Fig. 2(c) (for  $V_g = -100$  V) describe well the measured data for temperatures at high temperature (roughly above 70 K, see supplementary information<sup>41</sup>). At lower temperatures, by comparison, there is a notable deviation at low B-fields, which is due to the fact that the model does not include the weak anti-localization effect. From the fits, bulk carrier densities of  $5.3 \times 10^{23} \text{ m}^{-3}$  at 193 K and  $4.7 \times 10^{22} \text{ m}^{-3}$  at 70 K were calculated. This decrease upon cooling is in qualitative agreement with the assumed thermally activated behavior, and the absolute values are similar to those reported for  $\text{Bi}_2\text{Se}_3$  nanostructures.<sup>38</sup> Moreover, the obtained gap and bulk state resistance values are consistent with the fitting results based upon Eqs. (2)–(4) (see supplementary information).

In order to determine the nature of gap state, we further analyze the weak anti-localization (WAL) effect around zero B-field, which is notably enhanced with increasingly negative gate voltage (see Figs. 1(a) and 1(b)). The low field anomaly in the magneto-conductivity of  $\text{Bi}_2\text{Se}_3$  is well

described by the Hikami-Larkin-Nagaoka (HLN)<sup>42</sup> equation which assumes surface-state governed charge transport

$$\Delta\sigma(B) = -\alpha \cdot \frac{e^2}{\pi h} \left[ \psi \left( \frac{1}{2} + \frac{B_\phi}{B} \right) - \ln \left( \frac{B_\phi}{B} \right) \right], \quad (8)$$

where  $\alpha$  is a constant whose value depends on the involved surfaces ( $\alpha = 1/2$  if only one surface contributes,  $\alpha = 1$  if both the top and bottom surface conduct),  $\Delta\sigma(B) = \sigma(B) - \sigma(0)$  is the variation of 2-D magneto-conductivity, obtainable by multiplying the conductance with the geometric factor  $L/W = 1/3$ ,  $\psi$  is the digamma function, and  $B_\phi = \frac{\hbar}{4e l_\phi}$  is an effective magnetic field related to the dephasing length  $l_\phi$ . Previous magnetotransport studies on  $\text{Bi}_2\text{Se}_3/\text{Bi}_2\text{Te}_3$  grown by molecular beam epitaxy have concluded that only the top surface of the layer conducts.<sup>20,36</sup> By contrast, magnetotransport data gained from exfoliated  $\text{Bi}_2\text{Se}_3$  sheets have pointed toward both surfaces contributing to the transport.<sup>38</sup> In Fig. 3(a),  $\Delta\sigma(B)$  is plotted for the above sample under different applied gate voltages. The data can be well fitted using the HLN equation, which underscores that the gap state is the topological surface state of  $\text{Bi}_2\text{Se}_3$ . It is apparent that  $\alpha$  increases from 0.6 at  $V_g = 0$  V to 1.2 at  $V_g = -80$  V as seen in Fig. 3(b), suggesting that under the latter condition, charge transport occurs through both surfaces. The fact that  $\alpha$  slightly exceeds the value of 1 might be due to a residual contribution of the bulk state or to the rough estimation of sample geometry. The dephasing length  $l_\phi$  shows an initial increase upon changing the gate voltage from 0 V to  $-40$  V, which likely reflects the suppression of the bulk conduction band contribution. The subsequent decrease of  $l_\phi$  when the gate voltage is made more negative is ascribable to enhanced electron-electron interaction with decreasing electron density.<sup>20</sup>

The finding of gate-controllable LMR in  $\text{Bi}_2\text{Se}_3$  has implications for related materials such as  $\text{Ag}_{2+\delta}\text{Te}$  and  $\text{Ag}_{2+\delta}\text{Se}$ , which according to theory are likely candidates as TIs.<sup>31</sup> The MR in these compounds shows a transition from quadratic to linear B-field dependence at a certain crossover field.<sup>5,6</sup> Thus far, the physical meaning of this field has not been fully clarified. Specifically, within the quantum magnetoresistance model by Abrikosov it corresponds to the B-field above which all the electrons condense into the first

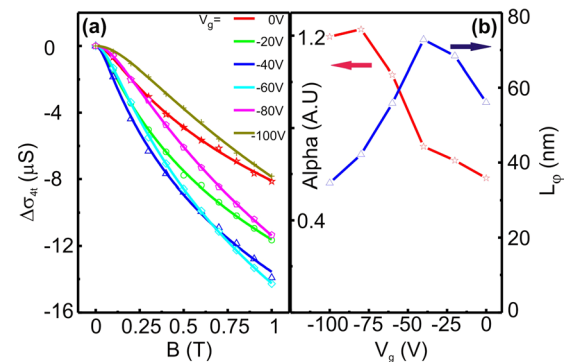


FIG. 3. (a) Anomaly in the two-dimensional magnetoconductivity, defined as  $\Delta\sigma_{4t}(B) = \sigma_{4t}(B) - \sigma_{4t}(0)$ , for different gate voltages applied to the same sample as in Figs. 1 and 2. The raw data are represented by symbols and the fitting curves by the solid lines. (b) Fitting parameter  $\alpha$  and dephasing length  $l_\phi$  as a function of gate voltage, both extracted from the line fits in (a).

Landau level,<sup>43,44</sup> while the classical Parish-Littlewood model considers it as a measure of average mobility or mobility disorder.<sup>45</sup> Based upon the above analysis, the crossover field may well reflect the competition between the bulk and topological surface state contributions.

In conclusion, we have demonstrated that by the application of high negative gate voltages to thin Bi<sub>2</sub>Se<sub>3</sub> plates, the B-field dependence of magnetoresistance can be tuned from quadratic to linear. This transition is accompanied by a notable enhancement of the weak anti-localization effect, while the temperature dependence of the sample resistance changes from metallic to semiconductor-like. Our data analysis suggests that the quadratic B-field dependence originates from the bulk conduction band, and the linear B-field dependence is most likely associated with the topologically protected surface state of the sheets. The possibility of gate control over the magnetotransport characteristics of thin topological insulator sheets could prove useful for the development of magnetic sensors.

We acknowledge H. Benia, C. Ast, and J. Honolka for valuable discussions and are grateful to T. Dufaux, A. Sagar, and Y. Weng (TEM studies) for experimental support.

- <sup>1</sup>P. Kapitza, *Proc. R. Soc. London, Ser. A* **119**(782), 358 (1928).
- <sup>2</sup>J. S. Lass, *J. Phys. C* **3**, 1926 (1970).
- <sup>3</sup>F. R. Fickett, *Phys. Rev. B* **3**, 1941 (1971).
- <sup>4</sup>*Colossal Magnetoresistive Oxides*, edited by Y. Tokura (Gordon and Breach Science, New York, 2000).
- <sup>5</sup>R. Xu, A. Husmann, T. F. Rosenbaum, M.-L. Saboungi, J. E. Enderby, and P. B. Littlewood, *Nature* **390**, 57 (1997).
- <sup>6</sup>M. von Kreutzbruck, G. Lembke, B. Mogwitz, C. Korte, and J. Janek, *Phys. Rev. B* **79**, 035204 (2009).
- <sup>7</sup>H. G. Johnson, S. P. Bennett, R. Barua, L. H. Lewis, and D. Heiman, *Phys. Rev. B* **82**, 085202 (2010).
- <sup>8</sup>J. Hu and T. F. Rosenbaum, *Nature Mater.* **7**, 697 (2008).
- <sup>9</sup>A. L. Friedman, J. L. Tedesco, P. M. Campbell, J. C. Culbertson, E. Aifer, F. K. Perkins, R. L. Myers-Ward, J. K. Hite, C. R. Eddy, Jr., G. G. Jernigan, and D. K. Gaskill, *Nano. Lett.* **10**, 3962 (2010).
- <sup>10</sup>L. Fu and C. L. Kane, *Phys. Rev. B* **76**, 045302 (2007).
- <sup>11</sup>H. J. Zhang, C. X. Liu, X. L. Qi, X. Dai, Z. Fang, and S. C. Zhang, *Nat. Phys.* **5**, 438 (2009).
- <sup>12</sup>M. Z. Hasan and C. L. Kane, *Rev. Mod. Phys.* **82**, 3045 (2010).
- <sup>13</sup>D. Hsieh, D. Qian, L. Wray, Y. Xia, Y. S. Hor, R. J. Cava, and M. Z. Hasan, *Nature* **452**, 970 (2008).
- <sup>14</sup>D. Hsieh, Y. Xia, L. Wray, D. Qian, A. Pal, J. H. Dil, J. Osterwalder, F. Meier, G. Bihlmayer, C. L. Kane, Y. S. Hor, R. J. Cava, and M. Z. Hasan, *Science* **323**, 919 (2009).
- <sup>15</sup>Y. Xia, D. Qian, D. Hsieh, L. Wray, A. Pal, H. Lin, A. Bansil, D. Grauer, Y. S. Hor, R. J. Cava, and M. Z. Hasan, *Nat. Phys.* **5**, 398 (2009).
- <sup>16</sup>D. Hsieh, Y. Xia, D. Qian, L. Wray, J. H. Dil, F. Meier, J. Osterwalder, L. Patthey, J. G. Checkelsky, N. P. Ong, A. V. Fedorov, H. Lin, A. Bansil, D. Grauer, Y. S. Hor, R. J. Cava, and M. Z. Hasan, *Nature* **460**, 1101 (2009).
- <sup>17</sup>D. Hsieh, Y. Xia, D. Qian, L. Wray, F. Meier, J. H. Dil, J. Osterwalder, L. Patthey, A. V. Fedorov, H. Lin, A. Bansil, D. Grauer, Y. S. Hor, R. J. Cava, and M. Z. Hasan, *Phys. Rev. Lett.* **103**, 146401 (2009).
- <sup>18</sup>Y. L. Chen, J.-H. Chu, J. G. Analytis, Z. K. Liu, K. Igarashi, H.-H. Kuo, X. L. Qi, S. K. Mo, R. G. Moore, D. H. Lu, M. Hashimoto, T. Sasagawa, S. C. Zhang, I. R. Fisher, Z. Hussain, and Z. X. Shen, *Science* **329**, 659 (2010).
- <sup>19</sup>Y. Zhang, K. He, C. Z. Chang, C. L. Song, L. L. Wang, X. Chen, J. F. Jia, Z. Fang, X. Dai, W. Y. Shan, S. Q. Shen, Q. Niu, X. L. Qi, S. C. Zhang, X. C. Ma, and Q. K. Xue, *Nat. Phys.* **6**, 584 (2010).
- <sup>20</sup>J. Chen, H. J. Qin, F. Yang, J. Liu, T. Guan, F. M. Qu, F. M. Zhang, J. R. Shi, X. C. Xie, C. L. Yang, K. H. Wu, Y. Q. Li, and L. Lu, *Phys. Rev. Lett.* **105**, 176602 (2010).
- <sup>21</sup>H. L. Peng, K. J. Lai, D. S. Kong, S. Meister, Y. L. Chen, X. L. Qi, S. C. Zhang, Z. X. Shen, and Y. Cui, *Nature Mater.* **9**, 225 (2010).
- <sup>22</sup>F. X. Xiu, L. He, Y. Wang, L. N. Cheng, L. T. Chang, M. R. Lang, G. Huang, X. F. Kou, Y. Zhou, X. W. Jiang, Z. G. Chen, J. Zou, A. Shailos, and K. L. Wang, *Nat. Nanotechnol.* **6**, 216 (2010).
- <sup>23</sup>D. X. Qu, Y. S. Hor, J. Xiong, R. J. Cava, and N. P. Ong, *Science* **329**, 821 (2010).
- <sup>24</sup>Z. Ren, A. A. Taskin, S. Sasaki, K. Segawa, Y. Ando, *Phys. Rev. B* **82**, 241306 (2010).
- <sup>25</sup>J. G. Checkelsky, Y. S. Hor, M. H. Liu, D. X. Qu, R. J. Cava, and N. P. Ong, *Phys. Rev. Lett.* **103**, 246601 (2009).
- <sup>26</sup>T. Hanaguri, K. Igarashi, M. Kawamura, H. Takagi, and T. Sasagawa, *Phys. Rev. B* **82**, 081305 (2010).
- <sup>27</sup>P. Cheng, C. L. Song, T. Zhang, Y. Y. Zhang, Y. L. Wang, J. F. Jia, J. Wang, Y. Y. Wang, B. F. Zhu, X. Chen, X. C. Ma, K. He, L. L. Wang, X. Dai, Z. Fang, X. C. Xie, X. L. Qi, C. X. Liu, S. C. Zhang, and Q. K. Xue, *Phys. Rev. Lett.* **105**, 076801 (2010).
- <sup>28</sup>J. G. Analytis, R. D. McDonald, C. Riggs, J. H. Chu, G. S. Boebinger, and I. R. Fisher, *Nat. Phys.* **6**, 960 (2010).
- <sup>29</sup>H. Tang, D. Liang, R. L. J. Qiu, and X. P. A. Gao, *ACS. Nano* **5**(9), 7510 (2011).
- <sup>30</sup>N. P. Butch, P. Syers, K. Kirshenbaum, A. P. Hope, and J. Paglione, *Phys. Rev. B* **84**, 220504 (2011).
- <sup>31</sup>W. Zhang, R. Yu, W. X. Feng, Y. G. Yao, H. M. Weng, X. Dai, and Z. Fang, *Phys. Rev. Lett.* **106**, 156808 (2011).
- <sup>32</sup>H. T. He, B. K. Li, H. C. Liu, X. Guo, Z. Y. Wang, M. H. Xie, and J. N. Wang, *Appl. Phys. Lett.* **100**, 032105 (2012).
- <sup>33</sup>D. S. Kong, W. H. Dang, J. J. Cha, H. Li, S. Meister, H. L. Peng, Z. F. Liu, and Y. Cui, *Nano Lett.* **10**, 2245 (2010).
- <sup>34</sup>H. Okamoto, *J. Phase Equilib.* **15**, 195 (1994).
- <sup>35</sup>W. Richter and C. R. Becker, *Phys. Status Solidi B* **84**, 619 (1977).
- <sup>36</sup>H. T. He, G. Wang, T. Zhang, I. K. S., G. K. L. Wong, and J. N. Wang, *Phys. Rev. Lett.* **106**, 166805 (2011).
- <sup>37</sup>J. L. Olsen, *Electron Transport in Metals* (Interscience, New York, 1962).
- <sup>38</sup>J. G. Checkelsky, Y. S. Hor, R. J. Cava, and N. P. Ong, *Phys. Rev. Lett.* **106**, 196801 (2011).
- <sup>39</sup>S. Giraud, A. Kundu, and R. Egger, *Phys. Rev. B* **85**, 035441 (2012).
- <sup>40</sup>M. H. Liu, C. Z. Chang, Z. C. Zhang, Y. Zhang, W. Ruan, K. He, L. L. Wang, X. Chen, J. F. Jia, S. C. Zhang, Q. K. Xue, X. C. Ma, and Y. Y. Wang, *Phys. Rev. B* **83**, 165440 (2011).
- <sup>41</sup>See supplementary material at <http://dx.doi.org/10.1063/1.4719196> for detailed discussions of the fitting results.
- <sup>42</sup>S. Hikami, A. I. Larkin, and Y. Nagaoka, *Prog. Theor. Phys.* **63**, 707 (1980).
- <sup>43</sup>A. A. Abrikosov, *Phys. Rev. B* **58**, 2788 (1998).
- <sup>44</sup>A. A. Abrikosov, *Europhys. Lett.* **49**, 789–793 (2000).
- <sup>45</sup>M. M. Parish and P. B. Littlewood, *Nature* **426**, 162 (2003).